Using Nanoparticle Optics Assay for Direct Observation of the Function of Antimicrobial Agents in Single Live Bacterial Cells†

Sophia V. Kyriacou, William J. Brownlow, and Xiao-Hong Nancy Xu*

Department of Chemistry & Biochemistry, Old Dominion University, Norfolk, Virginia 23529

Received June 27, 2003; Revised Manuscript Received November 1, 2003

ABSTRACT: Multidrug resistance (MDR) has been reported in both prokaryotes and eukaryotes, underscoring the challenge of design and screening of more efficacious new drugs. For instance, the efflux pump of *Pseudomonas aeruginosa* (gram-negative bacteria) can extrude a variety of structurally and functionally diverse substrates, which leads to MDR. In this study, we present a new platform that studies modes of action of antibiotics in living bacterial cells (*P. aeruginosa*), in real-time, at nanometer scale and single-cell resolution using nanoparticle optics and single living cell imaging. The color index of silver (Ag) nanoparticles (violet, blue, green, and red) is used as the sized index (30 ± 10, 50 ± 10, 70 ± 10, and 90 ± 10 nm) for real-time measurement of sized transformation of the cell wall and membrane permeability at the nanometer scale. We have demonstrated that the number of Ag nanoparticles accumulated in cells increases as the aztreonam (AZT) concentration increases and as incubation time increases, showing that AZT induces the sized transformation of membrane permeability and the disruption of the cell wall. The results demonstrate that nanoparticle optics assay can be used as a new powerful tool for real-time characterization of modes of action of antimicrobial agents in living cells at the nanometer scale. Furthermore, studies of mutants of WT bacteria (nalB-1 and ΔABM), suggest that an efflux pump (MexA−MexB−OprM) effectively extrudes substrates (nanoparticles) out of the cells, indicating that the MDR mechanism involves the induction of changes in membrane permeability and the intrinsic pump machinery.

Pseudomonas (P.) aeruginosa,[1] a gram-negative bacterium, has become a major opportunistic human pathogen and the leading cause of nosocomial infections in cancer, transplantation, burn, and cystic fibrosis patients (*1*−*3*). These infections are impossible to eradicate in part due to its renowned intrinsic resistance to a wide spectrum of structurally and functionally diverse antibiotics (*1*−*5*). To effectively treat the bacterial infections and prevent bacteria from developing multidrug resistance (MDR), the main strategy is to fully understand MDR mechanisms and carefully design and screen more efficacious new antibiotics. Recent studies reveal that the intrinsic resistance in *P. aeruginosa* is attributable to a synergy of low outer membrane permeability and active drug extrusion (*1*−*7*). Several efflux systems including MexA−MexB−OprM, MexCD−OprJ, MexEF−OprN and MexXY−OprM, have been reported in *P. aeruginosa* (*5*−*6*). The MexA−MexB−OprM pump is the major efflux pump in wild-type (WT) *P. aeruginosa*. This pump consists of two inner membrane proteins (MexA and MexB) and one outer membrane protein (OprM) (*8*−*9*). The MexB protein is believed to extrude the xenobiotics utilizing a proton motive force as an energy source (*7*−*9*). Despite extensive research over decades, the mechanisms of MDR still remain incompletely understood (*1*−*3*).

Currently, most methods used for the study of bacterial MDR mechanisms measure the accumulation of quinolone antibiotics in bacteria using radioactive labeled (^{14}C and ^{3}H) quinolones or natural fluorescent quinolones (*10*). Given that a common characteristic of MDR in bacteria (*P. aeruginosa*) is their broad resistance to quinolones, time courses of fluorescence intensity of quinolones (e.g., ethidium bromide) have been widely used as a popular means for real-time monitoring of the accumulation of substrates in bulk bacterial cells and used for assessing MDR (*10*−*14*). Such an approach provides an average accumulation (uptake and efflux) kinetic for a large population of cells. Individual cells, however, act independently and have unsynchronized membrane permeability, uptake, and efflux kinetics (*15*, *16*). Thus, the kinetics of uptake and efflux of substrates by individual cells are different from one another. Therefore, the uptake and efflux kinetics of an individual cell are lost in bulk measurement, which uses ensemble average means (*15*, *16*). Furthermore, such bulk measurements using time courses of fluorescence intensity of quinolones cannot provide insights into the sized transformation of membrane pores in intact cells. Thus, such bulk measurements cannot address several important questions, such as when and where the substrates induce the transformation of membrane permeability and efflux machinery, which lead to the MDR.

Many quantitative and qualitative methods have been developed to study antibiotic resistance levels in bacteria.

† This work was supported in part by NIH (RR15057-01), Old Dominion University, in the form of a start-up fund, and the Amideast Scholarship and Starr Foundation Scholarship (S.V.K.).

* To whom correspondence should be addressed. E-mail: xhxu@odu.edu. Web: www.odu.edu/sci/xu/xu.htm; Tel/fax: (757) 683−5698.

[1] Abbreviations: Ag, silver; AZT, aztreonam; EtBr, ethidium bromide; MDR, multidrug resistance; MIC, minimum inhibitory concentration; ms, millisecond; nm, nanometer; OD, optical density; *P. pseudomonas*; SPRS, surface plasma resonance spectra; TEM, transmission electron microscope; WT, wild-type.

10.1021/bi0351110 CCC: $27.50
Published on Web 12/09/2003

The most common techniques for the study of the susceptibility of bacteria to antibiotics are broth dilution and agar plate techniques (*17*). Both methods are used to determine the minimum inhibitory concentration (MIC) of antibiotics toward bacteria. Other techniques including efficacy time index (ETI) assay (*18*), time-kill analysis (*19*), double-disc synergy test (DDST) (*20*), inhibitor-potentiated disc diffusion test (IPDDT) (*20*), three-dimensional test (TDT) (*21*), and PCR/Nhe I test (*21*), have been used to measure the MIC and determine the susceptibility of bacteria. There is a range of specificity and sensitivity in these techniques. Some methods give false negative results. In addition, these methods are laborious and time-consuming. Furthermore, these methods cannot offer real-time temporal information for direct observation of the intrinsic resistance mechanisms of bacteria, the sized transformation of membrane pores, and the inhibitory mechanism of antibiotics in individual living cells. This hinders the further understanding of the modes of action of antimicrobial agents and the rational design of efficacious drugs to treat infections. Therefore, it is critical to develop a real-time screening tool that will provide real-time temporal and sized resolution for direct observation of modes of action of antimicrobial agents in individual living cells. Such a tool will aid to discover when and where the inhibitory mechanisms occur in living cells, permit one to better evaluate the pharmacokinetics of antibiotics, and offer new insights into possible regulatory pathways involved in MDR.

To this end, we have developed single nanoparticle optics assays and single living cell imaging to study the real-time sized transformation of cell wall and membrane permeability in individual living cells at nanometer (nm) sized resolution and millisecond (ms) temporal resolution. In this study, we demonstrate that single nanoparticle optics can be used to monitor inhibitory mechanisms of antimicrobial agents in individual living cells at the nanometer scale, and in real time. It is well-known that aztreonam (AZT) inhibits bacterial growth by interruption of the cell wall synthesis (*11*). Thus, we select AZT, a monocyclic β-lactam antibiotic, as an example to validate this new real-time nanoparticle optics assay. Furthermore, it has been widely reported that an efflux pump (MexA−MexB−OprM) can extrude a broad spectrum of substrates (*1*−*9*). Thus, we investigate the role of the efflux pump (MexA−MexB−OprM) in controlling the accumulation of substrates (EtBr, nanoparticles) in *P. aeruginosa* using nanoparticle optics.

MATERIALS AND METHODS

Silver Nanoparticle Preparation and Characterization. Silver nanoparticles are prepared by reducing 500 mL of 1 mM $AgNO_3$ aqueous solution using 10 mL of 1% fresh sodium citrate aqueous solution as described previously (*22*, *23*). The Ag nanoparticles are characterized by optical dark-field microscopy and spectroscopy, and transmission electron microscopy (TEM, JEOL 100CX), showing that the average sizes of nanoparticles are at 48 ± 15 nm (*22*). Samples for TEM imaging are prepared on 100 mesh Formvar coated copper grids (Electron Microscopy Sciences). Ag nanoparticle concentration is determined as 4×10^{-10} M by dividing the moles of nanoparticles by the volume of the solution. The moles of nanoparticles are calculated as follows. The volume of generated Ag is calculated by dividing the weight of Ag generated from the complete reduction of $AgNO_3$ by the density of silver (10.49 g/cm^3). The number of average size of Ag nanoparticles (48 nm) in the solution is computed by dividing the volume of generated Ag with the volume of individual Ag nanoparticles. The moles of Ag nanoparticles are then determined by dividing the number of Ag nanoparticles with Avogadro's constant (6.02×10^{23}).

Chemicals and Supplies. Stock solutions of 50 and 500 μg/mL AZT are prepared by dissolving AZT powder in saturated sodium bicarbonate solution and by diluting AZT solution with ultrapure water (Nanopore, 18 MΩ, sterilized) to the desired concentrations (*11*, *24*). Ethidium bromide (EtBr) stock solution is prepared in ultrapure water and the resulting solution is triple filtered using 0.2 μm sterilized membrane filters (Costar). Quartz slides ($25 \times 75 \times 1$ mm) and coverslips ($22 \times 30 \times 0.08$ mm) are purchased from VWR. 50 mM PBS buffer solution (150 mM NaCl at pH = 7.0) is prepared using ultrapure water. All chemicals including sodium citrate, ethidium bromide (EtBr), and silver nitrate ($AgNO_3$) are purchased from Sigma and used without any further purification or treatment.

Cell Culture and Preparation. Three strains of *P. aeruginosa*, WT (PAO4290, the strain that expresses the wide-type level of MexA−MexB−OprM), nalB-1 (TNP030#1, a mutant that overexpresses MexA−MexB−OprM), and ΔABM (TNP076, a mutant devoid of MexA−MexB−OprM), are used (*12*, *13*, *25*). Cells are precultured in a test tube containing L-broth medium (pH = 7.2) of 1% tryptone, 0.5% yeast extract, and 0.5% NaCl. The test tube is then placed in a shaker (Lab-line Orbit Envivon-Shaker, 150 rpm and 37 °C) overnight to ensure the full growth of the cells. Cells are then cultured for an additional 8 h. The cultured cells are harvested by centrifugation at 7500 rpm (Beckman model J2-21 centrifuge, JA-14 rotor) at 23 °C for 10 min, triple washed with 50 mM PBS (pH = 7.0), and then suspended again in the same buffer at a cell concentration of $OD_{600\ nm}$ = 0.1 (optical density at 600 nm). Three milliliters of the cell solutions containing 1.3 pM Ag nanoparticles and 0, 3.13, 31.3 μg/mL AZT are prepared by mixing 2703 μL of the cell solution ($OD_{600\ nm}$ = 0.1) and 9.8 μL of 0.4 nM Ag nanoparticles with ultrapure water, 187.8 μL of 50 μg/mL AZT, and 187.8 μL of 500 μg/mL AZT, respectively. Three milliliters of the cell solutions containing 10 μM EtBr and 0, 3.13, 31.3 μg/mL AZT are prepared by mixing 2703 μL of the cell solution ($OD_{600\ nm}$ = 0.1) and 110 μL of 274 μM EtBr with ultrapure water, 187.8 μL of 50 μg/mL AZT, and 187.8 μL of 500 μg/mL AZT, respectively. A timer is used to record the incubation time.

Antibiotic Susceptibility Study. Susceptibility testing and determination of the MIC of AZT in the presence of 10 μM EtBr or 1.3 pM Ag nanoparticles are performed using both the broth dilution method and single living cell imaging. Cells are first precultured in L-broth medium as described previously and then cultured for an additional 8 h in the same medium containing AZT (0, 3.13, 15.7, 31.3 μg/mL) in the presence of 10 μM EtBr or 1.3 pM Ag nanoparticles. The optical density of a 10× dilution of the cultured cell suspension at 600 nm ($OD_{600\ nm}$) is measured to determine the proliferation of cells using an UV−visible spectrometer (Cary 2G, Varian). In addition, a 20 μL aliquot of each mixed solution is imaged in a microchannel using single living cell imaging to determine the number of cells in the solution.

Nanoparticle Optics and Single Living Cell Imaging. The dark-field optical microscope is equipped with an oil dark-field condenser (Oil 1.43−1.20, Nikon), a 100× objective (Nikon Plan fluor 100× oil, iris, S.L. N.A. 0.5−1.3, W.D. 0.20 mm), the microscopic illuminator (100 W halogen), a CCD camera (Micromax, 5 MHz Interline, PID 1030 × 1300, Roper Scientific) for high-speed and high-resolution cell imaging, and a color digital camera (Coolpix 990, Nikon) for real-color imaging. Both cameras are added onto the microscope through a quad-adapter (Nikon) for real-time imaging. A 20 μL aliquot of the cell solution containing 1.3 pM Ag nanoparticles and AZT (0, 3.13, 31.3 μg/mL) is added into a microchannel and directly imaged using a dark-field microscope equipped with a CCD camera and color digital camera. The sealed microchannel is constructed by sandwiching the solution between a microscope slide and a cover slip as described in detail in our previous publications (*14*−*16*).

Fluorescence Spectroscopic Measurements. Time courses of fluorescence intensity of EtBr at 590 nm are measured by a fluorescence spectrometer (Perkin-Elmer LS50B) using a time-drive mode with a 3 s data acquisition interval and a 488 nm excitation line. These time courses of fluorescence intensity are used for real-time monitoring of accumulation kinetics of EtBr in bulk living cells in the absence and presence of AZT (0, 3.13, 31.3 μg/mL). The result is used to validate the nanoparticle optics assay for real-time measurement of modes of action of antibiotics at the nanometer-sized resolution.

RESULTS

Real-Time Imaging of AZT Function Using Nanoparticle Optics. Silver nanoparticles with diameters of 20−100 nm (48 ± 15 nm) are synthesized as described previously (*22*, *23*). The broad spectrum of Ag nanoparticles is characterized using surface plasmon resonance spectra (SPRS) and transmission electron microscope (TEM) (*22*, *26*). The full-frame optical images of nanoparticle solutions in Figure 1A show that multicolors of single nanoparticles are present in the solution. TEM images in Figure 1B also indicate that Ag nanoparticles with a variety of sizes are present in the solution, showing that the majority of nanoparticles are spheres, while a very few nanoparticles are triangular and hexagonal. The color distribution of single nanoparticles from a 0.4 nM Ag nanoparticle solution measured using dark-field microscopy and spectroscopy is used to compare with the sized distribution of single nanoparticles from the same solution, determined by TEM. The results in Figure 1C indicate that the color index of violet, blue, green, and red is correlated with sized index of 30 ± 10, 50 ± 10, 70 ± 10, and 90 ± 10 nm, respectively. These unique characteristics of nanoparticles offer a new opportunity to use these nanoparticles for direct measurement of the sized transformation of membrane pores in living cells, with millisecond temporal resolution and nanometer-sized resolution, using optical microscopy and spectroscopy.

Images of the cells (nalB-1) incubated with Ag nanoparticles and AZT in the microchannel are directly recorded using dark-field optical microscopy and spectroscopy (Figure 2). The results show that more Ag nanoparticles are accumulated in the cells as the AZT concentration increases (Figure 2), suggesting that the size of membrane pores increases as AZT concentration increases. The images clearly illustrate the morphology of the cells, indicating that the cellular membrane is intact in the absence of AZT (Figure 2A), while the membrane becomes disrupted as the AZT concentration increases to 3.13 (Figure 2B) and 31.3 μg/mL (Figure 2C). Full-frame images in Figure 3 demonstrate that many single living cells (WT) can be monitored simultaneously at single cell resolution, showing that more Ag nanoparticles are observed in the cells (WT) as the AZT concentration increases. In the absence of AZT, very few Ag nanoparticles are accumulated in WT cells, and the number of Ag nanoparticles in the cells remains almost unchanged over time (Figure 4A,a). As the AZT concentration increases to 3.13 and 31.3 μg/mL, the accumulation rate of intracellular Ag nanoparticles increases 2.8- and 6-fold, respectively (Figure 4A,b,c), demonstrating that AZT induces real-time sized transformation of the cell wall and membrane permeability.

To investigate the role of the MexA−MexB−OprM efflux pump in controlling of the function of AZT, we study two mutants, nalB-1 (a mutant that overexpresses MexA−MexB−OprM) and ΔABM (a mutant devoid of MexA−MexB−OprM). In the absence of AZT, as observed in WT, very few nanoparticles are accumulated in nalB-1 and ΔABM. The number of the nanoparticles remains almost unchanged over time (Figures 4B,C,a). In 3.13 μg/mL AZT, unlike WT, very few Ag nanoparticles are observed in nalB-1, and the number of Ag nanoparticles in nalB-1 remains unchanged over time (Figure 4B,b). In contrast, the number of Ag nanoparticles accumulated in ΔABM increases proportionally with time (Figure 4C,b). In 31.3 μg/mL AZT, the number of Ag nanoparticles in nalB-1 and ΔABM increases with time rapidly as observed in WT. Taken together, the results suggest that MexA−MexB−OprM plays an important role in the accumulation of the nanoparticles in the cells. Among these three strains, the mutant that overexpresses MexA−MexB−OprM (nalB-1) accumulates the least number of Ag nanoparticles, whereas the mutant devoid of MexA−MexB−OprM (ΔABM) accumulates the greatest number of Ag nanoparticles, suggesting that MexA−MexB−OprM appears to effectively extrude nanoparticles out of the cells at low AZT concentrations (0−3.13 μg/mL), at which concentrations the cellular membrane is still intact and its permeability is low. At higher AZT concentration (31.3 μg/mL), the cellular wall is destroyed. Thus, the extrusion pump is unable to overcome an overflow of substrates (AZT and nanoparticles), and the number of Ag nanoparticles accumulated in any of these three strains increases rapidly with time, at a rate of 6−8-fold higher than in the absence of AZT.

Fluorescence Spectroscopic Measurements. To rule out possible steric and size effects of using a large size of Ag nanoparticles as a probe for the real-time measurement of function of AZT, the small molecule (EtBr) is used as a fluorescence probe for the real-time measurement of the accumulation of EtBr in intact bulk cells. In the absence of AZT, time courses of fluorescence intensity of EtBr in intact cells (all three strains) show that the fluorescence intensity of EtBr increases slightly with time at a rate of 2×10^{-3} s^{-1} (Figure 5a). As the AZT concentration increases from 0 to 3.13 μg/mL, among three strains, fluorescence intensity

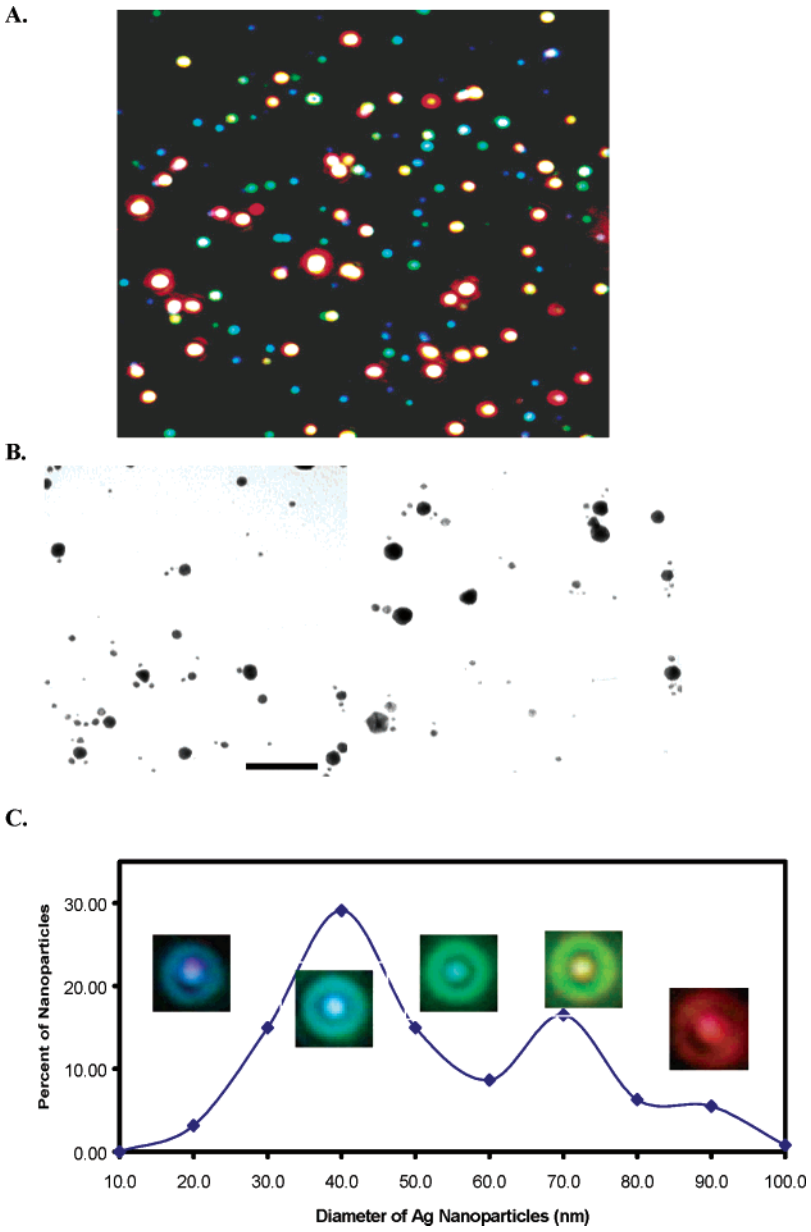

FIGURE 1: Determination of correlation between color index and sized index of Ag nanoparticles: (A) The representative optical image taken from a 0.4 nM Ag nanoparticle solution in a microchannel by a digital color camera through the dark-field optical microscope. The optical images of nanoparticles look larger than their actual sizes because of the optical diffraction limit (~200 nm). (B) Representative TEM images of Ag nanoparticles showing the sizes and shapes of nanoparticles. The scale bar represents 80 nm. (C) Cumulative histogram of the distribution of the number of Ag nanoparticles versus nanoparticle sizes with a cumulative interval at 10 nm (◆). The color distribution of Ag nanoparticles obtained from about 100 nanoparticles determined by the optical microscope in (A) is compared with the sized distribution of the nanoparticles measured by TEM in (B), suggesting that the color index of Ag nanoparticles can be used as the sized index with violet, blue, green, and red corresponding to 30 ± 10 (23%), 50 ± 10 (53%), 70 ± 10 (16%), and 90 ± 10 nm (8%), respectively. Optical images of single Ag nanoparticles are acquired in (A).

of EtBr in nalB-1 increases most slowly with time at a rate of 3×10^{-3} s^{-1}, whereas the fluorescence intensity of EtBr in ΔABM increases most rapidly with time at a rate of 0.1 s^{-1}. This result indicates that MexA−MexB−OprM appears to play a key role in the accumulation of EtBr in the cells in the absence and presence of 3.13 μg/mL AZT, suggesting that MexA−MexB−OprM effectively extrudes substrate (EtBr) out of the cells at low AZT concentrations (0−3.13 μg/mL). In 31.3 μg/mL AZT, fluorescence intensity of EtBr in all three strains increases rapidly with time at a rate of 0.1 s^{-1}. At such a high AZT concentration (31.3 μg/mL), the pump is unable to competitively extrude the overflow of EtBr that occurs as membrane permeability increases in the cells, owing to the disintegration of cell walls. This result agrees well with those observed using nanoparticle optics, demonstrating that the real-time nanoparticle optics assay is well suited for studying the function of antibiotics in living cells. Unlike bulk analysis using fluorescence spectroscopy, nanoparticle optics offers new insights into the sized transformation of cellular membranes in single living cells at the nanometer scale. For example, when the blue nanoparticles are accumulated inside the cells, the pores of membrane can be estimated at 50 ± 10 nm in diameter (*22*). When the green nanoparticles are observed inside the cells, the pores of membrane can be determined as 70 ± 10 nm in diameter (*22*).

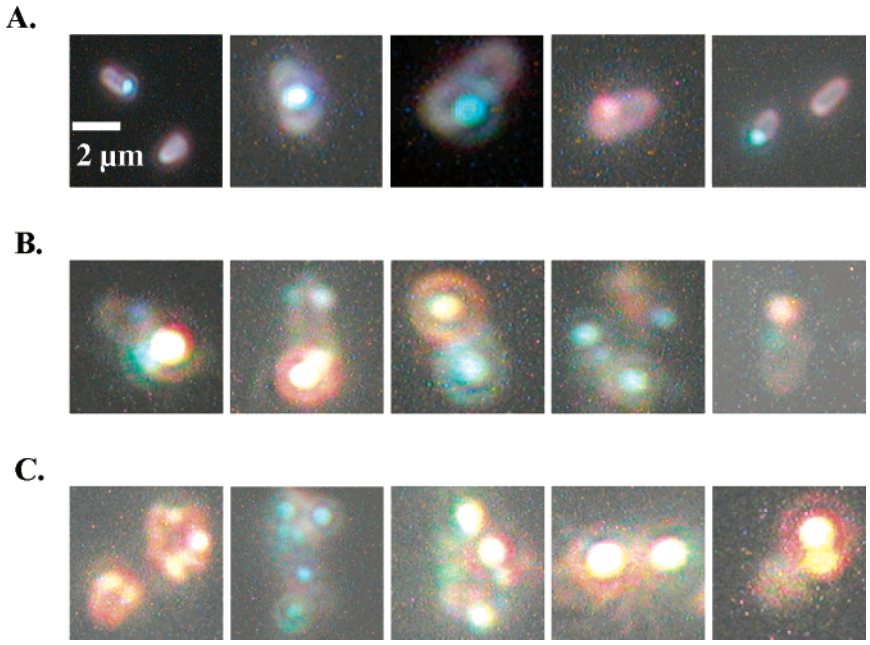

FIGURE 2: Direct observation of real-time sized transformation of membrane permeability in living cells (nalB-1) using single nanoparticle optics. Representative optical images (A−C) of single cells selected from ~60 cells in the full-frame images similar to Figure 3. The solutions containing the cells ($OD_{600\ nm} = 0.1$), 1.3 pM Ag nanoparticles, and (A) 0, (B) 3.13, and (C) 31.3 μg/mL AZT are prepared in a vial and imaged in a microchannel at a 15-min interval for 2 h, respectively.

Minimum Inhibitory Concentration (MIC). To ensure that 10 μM EtBr and 1.3 pM Ag nanoparticles do not compete with AZT for accumulation in the cells, we measured the MIC of AZT in the presence of 10 μM EtBr (Figure 6). The result indicates that the MIC of AZT in the presence of 10 μM EtBr or 1.3 pM Ag nanoparticles is the same as that observed in the absence of EtBr and Ag nanoparticles with the MIC of AZT at 3.13, 3.13, and 15.7 μg/mL for WT, ΔABM, and nalB-1, respectively, suggesting that the presence of 10 μM EtBr or 1.3 pM nanoparticles does not affect the accumulation of AZT in the cells. Furthermore, this result demonstrates that the presence of 10 μM EtBr or 1.3 pM Ag nanoparticles does not generate significant toxicity to the cells. These findings agree well with our previous measurements (*22*).

DISCUSSION

Optical properties (colors, SPRS) of Ag nanoparticles depend on size and shape of the nanoparticles and the dielectric constant of the embedded medium of the nanoparticles (*27*−*30*). Therefore, the colors of nanoparticles are associated with their sizes when the shape and embedded medium of nanoparticles remain unchanged. The colors (SPRS) of Ag nanoparticles are correlated with their sizes as shown in Figure 1 (*22*, *26*). Such unique features allow us to use the color index of nanoparticles (violet, blue, green, and red) as the sized index (30 ± 10, 50 ± 10, 70 ± 10, and 90 ± 10 nm) for the real-time measurement of sized transformation of cell wall and membrane permeability at the nanometer scale using dark-field optical microscopy.

The quantum yield of Rayleigh scattering of 20 nm Ag nanoparticles is about 10^7 times higher than that of a single fluorescent dye molecule (*27*−*30*). The scattering intensity of noble metal nanoparticles is proportional to the volume of nanoparticles (*27*−*30*). Thus, these Ag nanoparticles are extremely bright and are able to be directly observed using a dark-field microscope even with the unaided eye. Unlike fluorescent dyes, these nanoparticles do not suffer photodecomposition and can be used as probes to continuously monitor dynamic events in living cells for extended times. The scattering intensity of the nanoparticles decreases by about 10% as nanoparticles enter the cellular membrane because the cellular membrane and matrix absorb the light of the microscopic illuminator and reduce its intensity. In addition, the quantum yield of Rayleigh scattering of intracellular Ag nanoparticles is smaller than extracelluar Ag nanoparticles because intracellular Ag nanoparticles are surrounded by biomolecules (e.g., proteins, lipid) that reduce the reflection coefficient of Ag nanoparticles. Therefore, the nanoparticles outside the cellular membrane appear to radiate more sharply and brightly, whereas nanoparticles inside the cell membrane look blurry and dim (Figure 2). This feature allows us to determine whether the nanoparticles are inside or outside the cell membrane using optical microscopy (*22*, *26*). The locations of nanoparticles inside the cells have also been confirmed by TEM (*22*). The size of the nanoparticles (<100 nm) and the thickness of cell membrane (8 nm for inner or outer membrane and ~20 nm between inner and outer membrane of gram-negative bacteria) are below the optical diffraction limit (~200 nm). The scattering intensity of nanoparticles is much higher than that of cellular membrane because of the higher intrinsic optical dielectric constant of Ag nanoparticles. Therefore, the nanoparticles appear to be accumulated on the membrane, as shown in Figure 2. However, those nanoparticles are blurry and dim; hence, they are inside the cells.

Images of intact cells in Figure 3 demonstrate that bulk cells are monitored simultaneously at single-cell resolution. A greater number of Ag nanoparticles is observed in the cells as AZT concentration increases and as the incubation time increases (Figures 3 and 4). These are bacterial cells (prokaryotes). Currently, there is no evidence available to

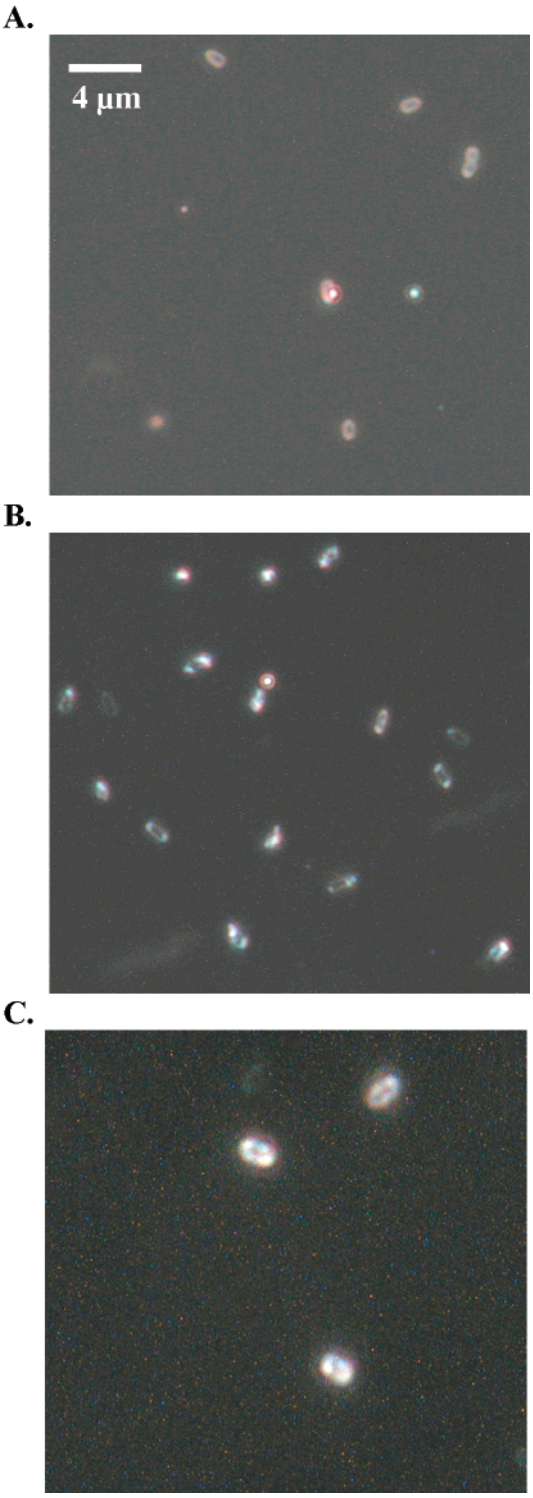

FIGURE 3: Real-time monitoring of membrane permeability of many single living cells (WT) simultaneously using nanoparticle optics. The full-frame optical images of the cells incubated with 1.3 pM Ag nanoparticles and (A) 0, (B) 3.13, and (C) 31.3 μg/mL of AZT in the microchannel, and directly recorded by the CCD camera (exposure time at 100 ms) and color digital camera through the dark-field optical microscope, showing that more nanoparticles are observed in the cells as the AZT concentration increases.

support the process of endocytosis or pinocytosis in prokaryotes (*P. aeruginosa*). Therefore, the increased accumulation of nanoparticles in the cells must be attributable to increased membrane permeability, suggesting that AZT induces real-time sized transformation of membrane pores and cell walls.

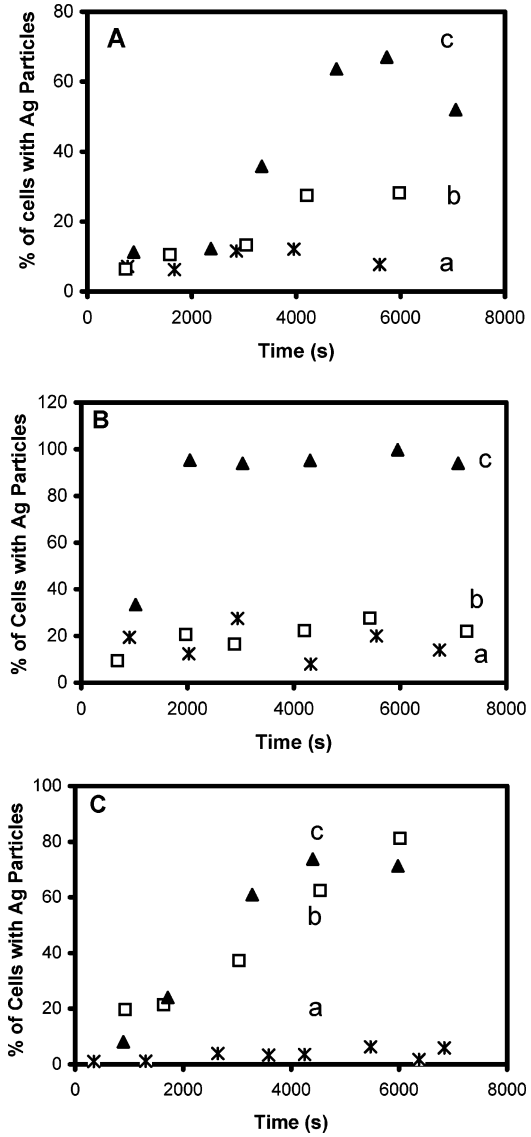

FIGURE 4: Direct observation of real-time sized transformation of membrane permeability of the cells induced by AZT. Plots of percent of the cells with Ag nanoparticles versus time: (A) WT, (B) nalB-1, and (C) ΔABM, from solutions containing the cells ($OD_{600\ nm}$ = 0.1), 1.3 pM Ag nanoparticles and (a, ∗) 0, (b, □) 3.13 and (c, ▲) 31.3 μg/mL of AZT. Ten images, similar to those in Figure 3, from each solution, are acquired at 15-min intervals with exposure time at 100 ms for each image. The 300 cells in total are analyzed for each data point.

Individual Ag nanoparticles can be well determined while the cellular membrane is still intact at the low AZT concentration (0−3.13 μg/mL) (Figure 2A,B). Optical images of nanoparticles always appear larger than their actual sizes because of the optical diffraction limit. However, the size of individual nanoparticles can be estimated using their optical colors (SPRS). At the high AZT concentration (31.3 μg/mL), the cellular membrane is disintegrated, which leads to a rapid accumulation of nanoparticles in the cells. The accumulation of intracellular Ag nanoparticles exceeds the capacity of the cells, and some of these nanoparticles begin to aggregate. Thus, it becomes difficult to distinguish individual nanoparticles (Figure 2C). For antibiotics (e.g., chloramphenicol) that do not cause the complete disruption of the cell wall, individual nanoparticles in single cells can be well distinguished and monitored over time (*22*). There-

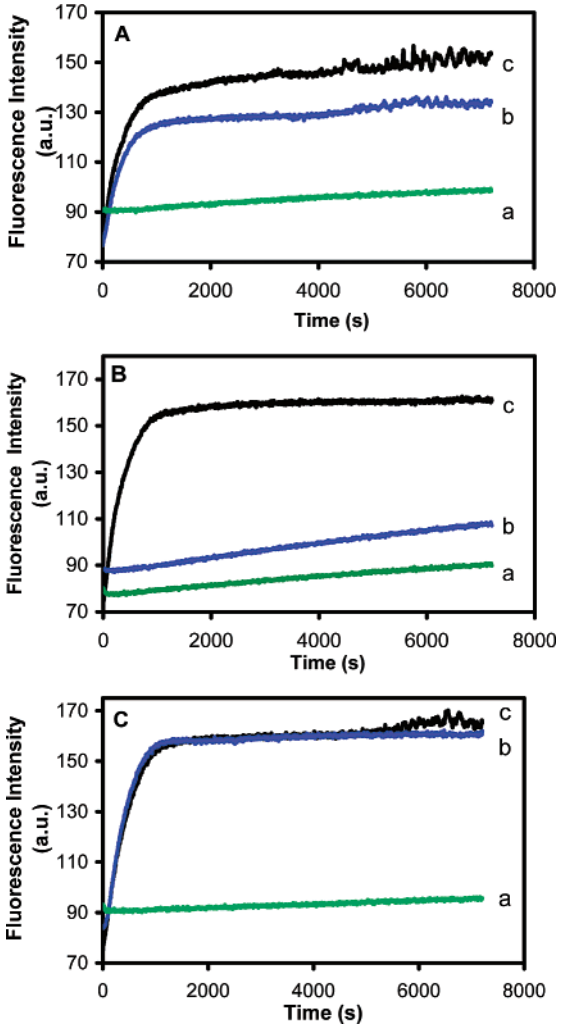

FIGURE 5: Real-time monitoring of accumulation kinetics of EtBr in the cells: representative time courses of fluorescence intensity of EtBr at 590 nm from the solutions containing 10 μM EtBr and the cells ($OD_{600\ nm}$ = 0.1): (A) WT, (B) nalB-1, and (C) ΔABM, and (a) 0, (b) 3.13, and (c) 31.3 μg/mL AZT, respectively. Time courses of fluorescence intensity are acquired from the 3.0 mL solution in a quartz cuvette by fluorescence spectroscopy using time-drive mode with a 3 s data acquisition interval and 488 nm excitation.

fore, the observation of aggregation of nanoparticles in living cells can be used to determine the complete disintegration of the cell membrane and cell wall, demonstrating another advantage of using nanoparticles as probes to study modes of action of antibiotics over fluorescent dyes, because fluorescence probes are unable to offer such information.

Two mutants of WT (nalB-1 and ΔABM) are also studied to determine the role of MexA−MexB−OprM in controlling the function of AZT. The results indicate that the membrane permeability of both mutants increases as AZT concentration increases and as incubation time increases, demonstrating that AZT induces the real-time transformation of membrane permeability of mutants. In 3.13 μg/mL AZT, the mutant that overexpresses MexA−MexB−OprM (nalB-1) accumulates the least number of Ag nanoparticles, whereas the mutant devoid of MexA−MexB−OprM (ΔABM) accumulates the greatest number of Ag nanoparticles. This result suggests that MexA−MexB−OprM plays an important role in the accumulation of Ag nanoparticles inside cells. *P. aeruginosa* is able to selectively extrude an array of

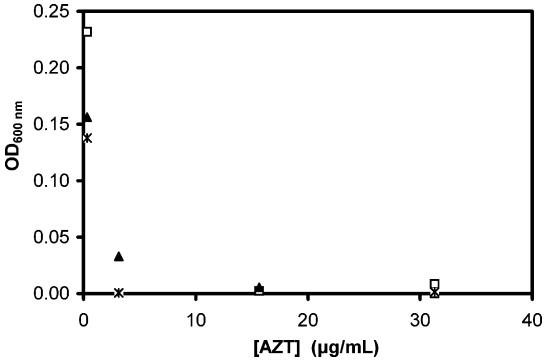

FIGURE 6: Determination of minimum inhibitory concentration (MIC) of AZT for ΔABM, WT, and nalB-1: representative plots of $OD_{600\ nm}$ versus the AZT concentration from the solutions containing 10 μM EtBr and ΔABM (□), WT (∗), and nalB-1 (▲) indicates that the MIC of ΔABM, WT, and nalB-1 is 3.13, 3.13, and 15.7 μg/mL, respectively. Similar results are observed when 10 μM EtBr is replaced by 1.3 pM Ag nanoparticles.

substrates, including antibiotics, dyes, detergents, and chemotoxic materials, out of the cells by efflux pumps using the proton motive force as the energy source (1−5). Thus, one plausible explanation for the role of MexA−MexB−OprM in the accumulation of the nanoparticles in the cells is that the pump extrudes nanoparticles out of cells. The mechanism of extrusion of nanoparticles could be similar to those of extrusion of other substrates. The details of how substrates are taken up and extruded by *P. aeruginosa* still remain unclear despite extensive studies over several decades (*1*−*5*). NalB-1, the mutant that overexpresses MexA−MexB−OprM, appears to extrude nanoparticles out of cells more effectively than ΔABM (mutant devoid of MexA−MexB−OprM). Consequently, nalB-1 accumulates fewer nanoparticles than ΔABM. In 31.3 μg/mL AZT, a significant number of Ag nanoparticles are accumulated in both mutants, indicating the complete disruption of membrane. This result demonstrates that the efflux pump (MexA−MexB−OprM) plays an important role in the equilibration of the sized transformation of membrane permeability only at low concentrations of AZT (0−3.13 μg/mL), when the membrane is still intact. This study also confirms that the function of AZT is indeed the destruction of cell membrane (Figures 2 and 3).

Comparison experiments using a small molecule (EtBr) as a fluorescence probe are carried out to validate a nanoparticle optics assay for direct observation of real-time function of AZT. EtBr has been a popular fluorescence probe for real-time monitoring of resistance mechanisms in bulk cells (*10*, *12*, *13*, *14*−*16*). EtBr is especially suitable to serve as a fluorescent probe for such studies because EtBr emits weaker fluorescence in an aqueous environment and becomes strongly fluorescent in nonpolar or hydrophobic environment, particularly as it enters cells and intercalates with DNA in cells (*31*). The accumulation kinetics of EtBr in cells, measured by time courses of fluorescence intensity of EtBr is comparable to the accumulation kinetics of intracellular Ag nanoparticles measured using single nanoparticle optics (Figures 4 and 5). Both measurements agree well. Therefore, both EtBr (10 μM) and Ag nanoparticles (1.3 pM) are reliable probes for the real-time study of function of AZT in living cells. The MIC of AZT in the absence and presence of EtBr (10 μM) or Ag nanoparticles (1.3 pM) remains unchanged

(Figure 6), suggesting that the presence of EtBr (10 μM) or Ag nanoparticles (1.3 pM) neither interferes with the accumulation of AZT in the cells nor creates significant toxicity to the cells.

CONCLUSION

Silver nanoparticle optics is developed and applied for real-time study of modes of action of an antibiotic (AZT) in living bacterial cells (*P. aeruginosa*). Real-time sized transformation of cell wall and membrane permeability induced by AZT is directly observed at the nanometer scale and at the single-cell resolution using single nanoparticle optics and single living cell imaging. The results suggest that AZT induces the real-time sized transformation of membrane permeability and disruption of the cell wall. This study demonstrates that noble metal nanoparticles can serve as a nonbleaching nanometer probe for real-time monitoring of function of antibiotics in single living cells at the nanometer scale for unlimited times. The real-time nanoparticle optics assay offers a rapid tool for real-time screening the function of antibiotics with millisecond temporal and nanometer-sized resolution, and provides a unique new opportunity for better evaluation of the pharmacokinetics of antibiotics. One can now use this new tool for real-time study of modes of action of other antibiotics in living cells for better characterization of their function, and for an advanced understanding of MDR mechanisms.

ACKNOWLEDGMENT

We thank Taiji Nakae (Tokai University School of Medicine, Japan) for the three strains of *Pseudomonas aeruginosa*.

REFERENCES

1. Poole, K. (2001) *J. Mol. Microbiol. Biotechnol. 3*, 255−264.
2. Nakae, T. (1997) *Microbiologia 13*, 273−284, and references therein.
3. Ryan, B. M., Dougherty, T. J., Beaulieu, D., Chuang, J., Dougherty, B. A., and Barrett, J. F. (2001) *Expert Opin. Invest. Drugs 10*, 1409−1422, and references therein.
4. Stover, C. K., Pham, X. Q., Erwin, A. L., Mizoguchi, S. D., Warrener, P., Hickey, M. J., Brinkman, F. S., Hufnagle, W. O., Kowalik, D. J., Lagrou, M., Garber, R. L., Goltry, L., Tolentino, E., Westbrock-Wadman, S., Yuan, Y., Brody, L. L., Coulter, S. N., Folger, K. R., Kas, A., Larbig, K., Lim, R., Smith, K., Spencer, D., Wong, G. K., Wu, Z., and Paulsen, I. T. (2000) *Nature 406*, 959−964.
5. Ma, D., Cook, D. N., Hearst, J. E., and Nikaido, H. (1994) *Trends Microbiol. 2*, 489−493.
6. Masuda, N., Sakagawa, E., Ohya, S., Gotoh, N., Tsujimoto, H., and Nishino, T. (2000) *Antimicrob. Agents Chemother. 44*, 3322−3327.
7. Lee, A., Mao, W., Warren, M. S., Mistry, A., Hoshino, K., Okumura, R., Ishida, H., and Lomovskaya, O. (2000) *J. Bacteriol. 182*, 3142−3150.
8. Maseda, H., Yoneyama, H., and Nakae, T. (2000) *Antimicrob. Agents Chemother. 44*, 658−664.
9. Morshed, S. R., Lei, Y., Yoneyama, H., and Nakae, T. (1995) *Biochem. Biophys. Res. Commun. 210*, 356−362.
10. Mortimer, P. G., and Piddock, L. J. (1991) *J. Antimicrob. Chemother. 28*, 639−653.
11. Greenwood, D. (1997) Modes of action in antibiotic and chemotherapy in *Antibiotic and Chemotherapy: Anti-infective Agents and Their Use in Therapy* (O'grady, F., Lambert, H. P., Finch, R. G., and Greenwood, D., Eds.) 7th ed., pp 10−21, Churchill Livingstone, New York.
12. Ocaktan, A., Yoneyama, H., and Nakae, T. (1997) *J. Biol. Chem. 272*, 21964−21969.
13. Yoneyama, H., Maseda, H., Kamiguchi, H., and Nakae, T. (2000) *J. Biol. Chem. 275*, 4628−4634.
14. Xu, X.-H. N., Wan, Q., Kyriacou, S., Brownlow, W., and Nowak, M. (2003) *Biochem. Biophys. Res. Commun. 305*, 941−949.
15. Kyriacou, S. V., Nowak, M. E., Brownlow, W. J., and Xu, X.-H. N. (2002) *J. Biomed. Opt. 7*, 576−586.
16. Xu, X.-H. N., Brownlow, W., Huang, S., and Chen, J. (2003) *Biochem. Biophys. Res. Commun. 305*, 79−86.
17. Andrews, J. M. (2001) *J. Antimicrob. Chemother. 48*, 5−16.
18. Okazaki, M., Suzuki, K., Asano, K., Shukuya, N., Egami, T., Higurashi, Y., Morita, K., Uchimura, H., and Watanabe, T. (2002) *J. Infect. Chemother. 8*, 37−42.
19. Fung-Tomc, J. C., Gradelski, E., Valera, L., Huczko, E., and Bonner, D. P. (2002) *Int. J. Antimicrob. Agents 20*, 57−60.
20. Palasubramaniam, S., and Parasakthi, N. (2001) *Malays. J. Pathol. 23*, 73−78.
21. Bedenic, B., Randegger, C., Boras, A., and Haechler, H. (2001) *Chemother. 13*, 24−33.
22. Xu, X.-H. N., Kyriacou, S., Brownlow, W., Wan, Q., and Viola, J., manuscript submitted.
23. Lee, P. C., and Meisel, D. (1982) *J. Phys. Chem. 86*, 3391−3395.
24. Ferraro, M. J., and Wikler, M. A. (2000) *NCCLS Methods for Dilution Antimicrobial Susceptibility Tests for Bacteria that Growth Aerobically*, 5th ed., Vol. 20, p 44, Ortho-McNeil, Raritan, NJ.
25. Saito, K., Yoneyama, H., and Nakae, T. (1999) *FEMS Microbiol. Lett. 179*, 67−72.
26. Xu, X.-H. N., Chen, J., Jeffers, R., and Kyriacou, S. (2002) *Nano Lett. 2*, 175−182.
27. Mulvaney, P. (1996) *Langmuir 12*, 788−800.
28. Bohren, C. F., and Huffman, D. R. (1983) *Absorption and Scattering of Light by Small Particles*, pp 287−380, Wiley, New York, and references therein.
29. Kreibig, U., and Vollmer, M. (1995) *Optical Properties of Metal Clusters*, pp 14−123, Springer, Berlin, and references therein.
30. Mie, G. (1908) *Beiträg zur Optik trüber Medien, speziell kolloidaler Metrallösungen Ann. Phys. 25*, 377−445.
31. Morgan, A. R., Lee, J. S., Pulleyblank, D. E., Murray, N. L., and Evans, D. H. (1979) *Nucleic Acids Res. 7*, 547−569.

BI0351110